Electron kinetic effects in plasma expansion and ion acceleration

T. Grismayer, P. Mora, J. C. Adam, and A. Héron
Centre de Physique Théorique, École Polytechnique, CNRS, 91128 Palaiseau, France
(Received 5 February 2008; published 30 June 2008)

The one-dimensional expansion of a plasma slab is studied using a kinetic description of the electrons based on an adiabatic invariant. The distribution function of the electrons is determined at any time and any position. Solution of the Poisson equation then enables us to determine the electric potential and the ion acceleration. Special attention is devoted to the disassembly time of the plasma slab which appears shorter than expected, due to the distortion of the electron distribution function. The spatial structures of the ion and electron densities and velocities are presented, together with a prediction of the maximum ion velocity. The model is compared to particle-in-cell simulations and excellent agreement is found.

DOI: 10.1103/PhysRevE.77.066407 PACS number(s): 52.38.Kd, 52.40.Kh, 52.65.Ww

I. INTRODUCTION

The quest for multi-MeV protons is at the forefront of the reasearch in laser-plasma physics [1–8]. These energetic ion beams have unique properties such as ultralow emittance and short duration and have opened up a way to several applications [9–11] such as proton therapy [12]. Several schemes have been proposed to generate such ions and the most frequently suggested assumes that ions are emitted from the rear surface of thin foils irradiated with short-pulse, ultrahigh-intensity lasers ($\tau \lesssim 1$ ps, $I\lambda^2 > 10^{18}$ W cm^{-2} μm^2). Hot electrons are accelerated by the laser pulse at the front surface, then propagate through the target, and form on the rear surface an electron sheath which accelerates ions [3,4,7,8,13–15]. Controlling the ion acceleration process and particularly the ion energy spectrum implies a good comprehension of the electron heating mechanism by the laser [16–18], the plasma expansion structure [19–24], the influence of the initial ion density profile [25], and the electron-ion energy transfer [21,26–28].

The electron cooling and the energy transfer in plasma expansion has been the subject of numerous studies. The energy exchange between electrons and ions in the self-similar expansion of a semi-infinite plasma was studied in Ref. [21]. Kinetic analytical solutions for the expansion of a Gaussian plasma in the quasineutral limit were given in Refs. [26,27]. More recently, Ref. [28] studied electron cooling in the expansion of a one-dimensional finite-size plasma with a hybrid model assuming a time-dependent Maxwell-Boltzmann distribution. In the present paper, we propose a method that treats the expansion of a finite plasma foil with a nonrelativistic kinetic description of the electrons, including the charge separation effect. The method is based on the time scale separation between the transit time of the electrons in the electric potential and the hydrodynamic time of the plasma [29,30]. It allows us to calculate with high accuracy and small computational effort the evolution of the electron distribution function during the expansion. When the initial ion density is spatially uniform within a finite size, we observe a strong distortion of the electron distribution function, with respect to a Maxwellian distribution, during the early stage of the plasma expansion.

The paper is organized as follows. In Sec. II we recall briefly the adiabatic invariant theory and how this theory can be used to calculate the energy variation of an electron in a potential slowly varying with time. For given analytical potentials, we calculate the corresponding electron energy variation and show in particular how the electron distribution function can be distorted from its initial shape in the self-similar potential corresponding to the early expansion of a plasma slab. In Sec. III we explicitly develop the analytical and numerical algorithm used to describe the one-dimensional expansion of a plasma slab. In particular, we describe a numerical code where ions are treated as particles (as in Ref. [28]), and where electrons are fully described by a slowly time-evolving distribution function. The numerical results of the code are shown in the last section and compared with the results of particle-in-cell (PIC) simulations and with the results of the hybrid model of Ref. [28]. We find excellent agreement with the PIC results. We describe the departure of the distribution function from a Maxwellian distribution and the evolution of the electron phase space. Special attention is given to the calculation of the ion acoustic speed in the present kinetic theory, and to its effect on the disassembly time of the plasma slab. We show that the rarefaction wave which travels at the ion acoustic speed toward the center of the foil accelerates due to the distortion of the electron distribution function, in contrast to the prediction of the hybrid model based on Maxwellian electron distribution functions [28]. The spatial profiles of the ion and electron densities and of the electrostatic field and potential are also displayed. Finally we compared the time evolution of the field and the velocity at the ion front to the ones we obtained in the hybrid model of Ref. [28].

II. ELECTRON KINETIC THEORY IN A SLOWLY TIME-VARYING POTENTIAL

On a time scale smaller that the inverse of the collision frequency, the one-dimensional nonrelativistic collective dynamic of the plasma electron population is governed by the Vlasov equation

$$\frac{\partial f_e}{\partial t} + v\frac{\partial f_e}{\partial x} + \frac{e}{m_e}\frac{\partial \Phi}{\partial x}\frac{\partial f_e}{\partial v} = 0, \tag{1}$$

where $f_e = f_e(x,v,t)$ is the electron distribution function. From kinetic theory, it is known that, if one can find some

motion invariants, then any function of these invariants is a solution of the Vlasov equation.

A. Adiabatic invariant

Our study deals with the expansion of a one-dimensional finite plasma slab, where the noncollisional electron gas is located in a self-consistent electrostatic potential well formed with ions of mass m_i and charge Ze. We assume a symmetric expansion around the position $x=0$, which is the position of the center of the slab. The potential satisfies at any time

$$\Phi(x=0,t)=0, \tag{2}$$

$$\Phi(x\to\pm\infty,t)\to-\infty, \tag{3}$$

$$\frac{\partial\Phi}{\partial x}(x\to\pm\infty,t)=0. \tag{4}$$

The second condition above ensures that there is no electron at infinity.

The potential is assumed to be a monotonic function of space for $|x|>0$ and to be slowly varying with time. Hence a time scale separation results from the condition

$$\frac{\mathcal{T}}{t_\Phi}=\mathcal{T}\left|\frac{1}{\Phi}\frac{\partial\Phi}{\partial t}\right|\ll 1, \tag{5}$$

with

$$\mathcal{T}=\sqrt{\frac{m_e}{2}}\oint\frac{dx}{\sqrt{\mathcal{E}+e\Phi}}, \tag{6}$$

where $\mathcal{T}$ is the electron period in the well, t_Φ is the characteristic time of variation of the electric potential, and $\mathcal{E}=\frac{1}{2}m_ev^2-e\Phi(x,t)$ is the total energy of an electron. The condition (5) is a consequence of the smallness of the ratio m_e/m_i, as t_Φ is proportional to $\sqrt{m_i/Z}$.

Following our assumptions, the invariant of the motion is known to be [29,32]

$$I=\oint p\,dx, \tag{7}$$

where $p=m_ev$ is the electron momentum and where the integral is computed along the electron trajectory, with values of $\mathcal{E}$ and Φ independent of time. Note that the adiabatic invariant I can be considered as a function of the energy and of the time, $I=I(\mathcal{E},t)$, the time dependence being due to the time dependence of the electric potential Φ.

B. Energy variation

To lowest order, the electron distribution function is a function of only the adiabatic invariant (7),

$$f_e=f_e[I(\mathcal{E},t)]. \tag{8}$$

We can rewrite the Vlasov equation by noticing that the electron distribution depends only on the energy and the time. After the corresponding change of variables, Eq. (1) reads

$$\frac{\partial f_e}{\partial t}-e\frac{\partial\Phi}{\partial t}\frac{\partial f_e}{\partial\mathcal{E}}=0. \tag{9}$$

The characteristics of (9) can be determined by averaging the energy variation rate over an electron period [29],

$$\left\langle\frac{d\mathcal{E}}{dt}\right\rangle=-e\left\langle\frac{\partial\Phi}{\partial t}\right\rangle=-e\frac{\oint\frac{\partial\Phi}{\partial t}\frac{dx}{\sqrt{\mathcal{E}+e\Phi}}}{\oint\frac{dx}{\sqrt{\mathcal{E}+e\Phi}}}. \tag{10}$$

One notices that the expression (10) is strictly equivalent to the equation $\langle dI/dt\rangle=0$. By definition, the solution of Eq. (10) allows one to solve the kinetic equation (9).

C. Examples with analytical potentials

1. Potential with uncoupled variables

First of all, we study the example of potentials that can be written in the form

$$e\Phi(x,t)=h(t)\Psi(x), \tag{11}$$

where h is a slowly time-varying function satisfying the adiabatic condition (5) and Ψ a monotonic function of space for $|x|\geq 0$. In the case of uncoupled variables, Eq. (10) reads

$$\left\langle\frac{d\mathcal{E}}{dt}\right\rangle=-e\frac{dh}{dt}\frac{\oint\Psi\frac{dx}{\sqrt{\mathcal{E}+e\Phi}}}{\oint\frac{dx}{\sqrt{\mathcal{E}+e\Phi}}}=\frac{1}{h}\frac{dh}{dt}\left(\mathcal{E}-\frac{I}{2\mathcal{T}}\right), \tag{12}$$

where the ratio $I/\mathcal{T}$ is *a priori* a function of $\mathcal{E}$ and t. One remarks that a distribution function, if initially Maxwellian, remains Maxwellian if the energy variation rate $d\mathcal{E}/dt$ is proportional to the energy. Thus, the potentials for which the ratio $I/\mathcal{T}$ is proportional to the energy conserve the Maxwell-Boltzmann equilibrium (with a time-dependent temperature). A trivial example is given by the slowly time-dependent harmonic oscillator for which the adiabatic invariant is well known [32], $I=\mathcal{E}\mathcal{T}$. However the harmonic oscillator potential is not the only one that satisfies the condition $I/\mathcal{T}\propto\mathcal{E}$. Let us assume that a potential may be written as $e\Phi(x,t)=h(t)\Psi(x)=-h(t)x^\alpha$, with $\alpha>0$. The invariant and the period of an electron read

$$I=4\sqrt{2m_e\mathcal{E}}\left(\frac{\mathcal{E}}{h}\right)^{1/\alpha}\mathcal{J}_\alpha, \tag{13}$$

$$\mathcal{T}=4\sqrt{\frac{m_e}{2\mathcal{E}}}\left(\frac{\mathcal{E}}{h}\right)^{1/\alpha}\mathcal{J}'_\alpha, \tag{14}$$

with $0<\mathcal{J}_\alpha=\int_0^1\sqrt{1-t^\alpha}dt<1$ and $\mathcal{J}'_\alpha=\int_0^1 1/\sqrt{1-t^\alpha}dt>1$. One deduces that the ratio between the invariant and the period is proportional to the energy,

$$\frac{I}{\mathcal{T}} = 2\frac{\mathcal{J}_\alpha}{\mathcal{J}'_\alpha}\mathcal{E}. \tag{15}$$

As a result, if the initial distribution is Maxwellian, it will remain Maxwellian for any time for such a power law potential.

2. Self-similar potential

Let us now consider the self-similar potential obtained in the quasineutral isothermal expansion of semi-infinite plasma [19], $e\Phi_{ss} = -k_B T_e(1 + x/c_s t)$. Here $x=0$ corresponds to the edge of the initial semi-infinite plama which occupies the $x<0$ half space, T_e is the electron temperature in the plasma, $c_s = (Zk_B T_e/m_i)^{1/2}$ is the ion acoustic velocity, and the ions are assumed to be cold. One can compute the energy variation of an electron during its transit in the potential,

$$\Delta\mathcal{E} = -\sqrt{\frac{em_e}{2}}\int_{-c_s t}^{x_r} \frac{\partial\Phi_{ss}}{\partial t}\frac{dx}{\sqrt{\mathcal{E} + e\Phi_{ss}}} \simeq \frac{4\sqrt{2}}{3}\sqrt{\frac{Zm_e}{m_i}}\sqrt{\frac{\mathcal{E}}{k_B T_e}}\left(\frac{3k_B T_e}{2} - \mathcal{E}\right). \tag{16}$$

The above expression (16) is identical to the one obtained in Ref. [21]. The time spent by the electron in the self-similar potential ($x > -c_s t$) is given by

$$\mathcal{T}_{ss} = 2\sqrt{\frac{m_e}{2}}\int_{-c_s t}^{x_r}\frac{dx}{\sqrt{\mathcal{E} + e\Phi_{ss}}} = \frac{4}{\sqrt{2}}\sqrt{\frac{Zm_e}{m_i}}\sqrt{\frac{\mathcal{E}}{k_B T_e}}t, \tag{17}$$

where x_r is the turning point of the electron.

For large enough values of the self-similar variable, $\xi = x/c_s t \gg 1$, the characteristic time of variation of the potential is $t_\Phi = |\Phi/\partial_t\Phi| \simeq t$. Thus, the condition (5), which reads here

$$\mathcal{E} \ll k_B T_e \frac{m_i}{Zm_e}, \tag{18}$$

is clearly satisfied.

The exact trajectories of a few electrons in the self-similar potential have been plotted in Fig. 1. In agreement with the expression (16), one can see that low-energy electrons ($\mathcal{E} < 3k_B T_e/2$) experience an energy gain whereas the high-energy ones ($\mathcal{E} > 3k_B T_e/2$) experience an energy loss. In any case the electrons gain energy when $x<0$ and lose energy when $x>0$.

If we consider now the expansion of a plasma slab of initial thickness L, with $L \gg c_s t \gg \lambda_{D0}$, where λ_{D0} is the Debye length in the unperturbed plasma, we can assume that the expansion on both sides of the slab is initially satisfactorily described by the self-similar solution, at least in the quasineutral part of the expansion [24]. In this limit, the electron period is given by

$$\mathcal{T} = 2\sqrt{\frac{m_e}{2\mathcal{E}}}(L - 2c_s t) + 2\mathcal{T}_{ss} \simeq 2\sqrt{\frac{m_e}{2\mathcal{E}}}L. \tag{19}$$

One thus finds that

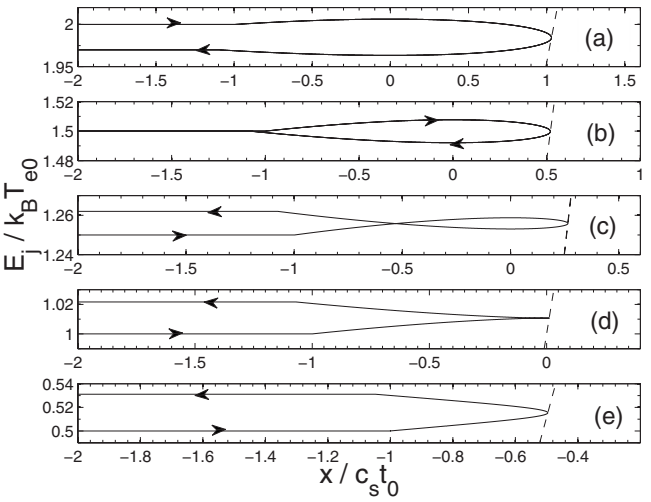

FIG. 1. Electron trajectories in a self-similar potential for different initial electron energies. The electron comes from the left and enters the potential at the position $x=-c_s t_0$ at time $t=t_0$. (a) $\mathcal{E} = 2k_B T_e$, $\Delta\mathcal{E}<0$. (b) $\mathcal{E}=3k_B T_e/2$, $\Delta\mathcal{E}=0$. (c) $\mathcal{E}=1.25k_B T_e$, $\Delta\mathcal{E}>0$. (d) $\mathcal{E}=-e\Phi_{ss}(0,t)=k_B T_e$, $\Delta\mathcal{E}>0$. (e) $\mathcal{E}=k_B T_e/2$, $\Delta\mathcal{E}>0$. The dashed lines correspond to the potential $-e\Phi_{ss}$ at the time when the electrons turn back.

$$\left\langle\frac{d\mathcal{E}}{dt}\right\rangle \simeq \frac{2\Delta\mathcal{E}}{\mathcal{T}} \simeq \frac{8}{3}\frac{c_s}{k_B T_e L}\mathcal{E}\left(\frac{3k_B T_e}{2} - \mathcal{E}\right). \tag{20}$$

The calculation of the electron energy variation in the linear self-similar potential, which is approximately valid for the initial phase of the slab expansion, reveals that the electron distribution function will be progressively distorted with respect to a Maxwellian distribution, evolving toward a super-Maxwellian (top-hat) distribution. (Note that this behavior is dependent on the initial conditions of the system, and that in the particular case of an initial Gaussian ionic density [31,33], the potential remains quadratic in the quasineutral part of the expansion, and thus the distribution function stays Maxwellian while cooling down).

III. ELECTRON KINETIC MODEL FOR PLASMA EXPANSION

A. Kinetic model

The electron distribution function distortion mentioned above can only be described by a kinetic approach, which is the subject of this section. In contrast with the hybrid model used in Ref. [28], where the electron distribution was assumed to be Maxwellian at any time, we do not make any prescription on the electron distribution function, except at the initial time $t=0$.

Initially, the ions are at rest and fill a foil of thickness L with an uniform density n_{i0}. Though the model can be run with any initial electron distribution function, in this paper we restrict our study to the case of an initial Maxwellian distribution, with temperature T_{e0}, with $v_{\mathrm{th}0} = (k_B T_{e0}/m_e)^{1/2}$ the corresponding thermal velocity. We also define $n_{e0} = Zn_{i0}$.

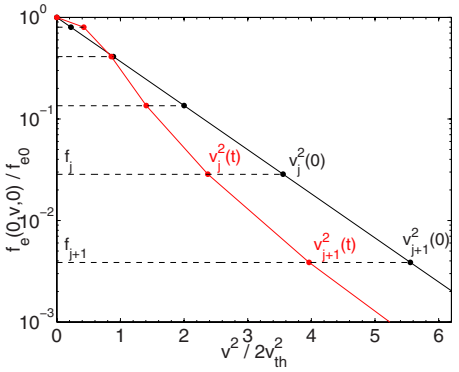

FIG. 2. (Color online) Discretization of the electron velocity distribution in the center of the foil, $x=0$. The initial distribution is plotted with black points, while the distribution at a time t is plotted with red points. The f_j remain constant during the expansion whereas the v_j evolve with time. The electron distribution is reconstructed with pieces of Maxwellian between each point.

The distribution function for the electrons is governed by Eq. (9). The ions are treated as particles and obey the equation of motion

$$\frac{dv_i}{dt} = -\frac{Ze}{m_i}\frac{\partial \Phi}{\partial x}. \tag{21}$$

The electrostatic potential is determined by the Poisson equation

$$\frac{\partial^2 \Phi}{\partial x^2} = \frac{e}{\epsilon_0}(n_e - Zn_i), \tag{22}$$

where

$$n_e(x,t) = \int_{-\infty}^{\infty} f_e dv, \tag{23}$$

and where the ion density is determined from the position of the ions.

The Vlasov equation (9) is solved by computing numerically the equation of the characteristics (10). The equation of the characteristics may be interpreted as a kinetic generalization of the time evolution of the electron temperature in the hybrid model used in Ref. [28]. In fact, the numerical resolution of the plasma expansion is similar to the one described in [28], with the electronic population now described by the distribution f_e. In practice, a finite number (between $n=10$ and 100) of characteristics are computed. Let $v_j(t)$ (for $j=0$ to $n-1$) be the absolute value of the velocity of the electron labeled j when it goes through the center of the foil ($x=0$), and f_j the value of the distribution function for this particular electron (as a property of the Vlasov equation, f_j does not vary with time). The electron distribution function is entirely defined by the functions $v_j(t)$ and by the knowledge of the electrostatic potential $\Phi(x,t)$. It is reconstructed in any position and at any time piece by piece as illustrated in Fig. 2, which shows an example of the discretization of the electron velocity distribution in the center of the foil ($x=0$) at two different times, including the initial time $t=0$, and as described more precisely in the next section.

B. Distribution function discretization

Let $\mathcal{E}_j(t)=m_e v_j(t)^2/2$ be the total energy of the electron labeled j. We assume that the electrons whose energy is between two successive quantities $\mathcal{E}_j(t)$ and $\mathcal{E}_{j+1}(t)$ are described by a piece of Maxwellian characterized by a temperature $T_j(t)$. As a result, the distribution function is written as a sum of Maxwell-Boltzmann distributions h_j in the following way:

$$f_e(x,v,t) = \sum_{j=0}^{\infty} h_j(x,v,t)\Pi_j(v,x). \tag{24}$$

The window functions Π_j are defined by

$$\Pi_j(v,x) = \mathcal{H}(v-u_j) - \mathcal{H}(v-u_{j+1}), \tag{25}$$

where $\mathcal{H}$ is the Heaviside function and the quantities u_j are given by

$$u_j(x,t) = \left(v_j^2(t) + \frac{2e\Phi(x,t)}{m_e}\right)^{1/2}. \tag{26}$$

Note that u_j corresponds to the velocity of the electron labeled j at position x in the plasma. The Maxwell-Boltzmann distributions are written as

$$h_j(x,v,t) = \alpha_j F_j(x,v,t) = \frac{\alpha_j n_{e0}}{\sqrt{2\pi}v_{\mathrm{th}0}} \exp\left(\frac{e\Phi}{k_B T_j}\right)\exp\left(\frac{-v^2}{2v_{\mathrm{th}j}^2}\right), \tag{27}$$

with

$$\alpha_j = f_j \exp\left(\frac{\mathcal{E}_j}{k_B T_j}\right), \tag{28}$$

where the f_j are the normalized values of the distribution function at the center of the foil,

$$f_j = f_e(x=0,v_j,t)\frac{\sqrt{2\pi}v_{\mathrm{th}0}}{n_{e0}}. \tag{29}$$

The temperatures T_j are defined in order to provide the continuity of $f_e(x,v,t)$, with

$$f_{j+1} = f_j \exp\left(\frac{\mathcal{E}_j - \mathcal{E}_{j+1}}{k_B T_j}\right). \tag{30}$$

Finally $v_{\mathrm{th}j}=(k_B T_j/m_e)^{1/2}$ is the thermal velocity associated with T_j.

The distribution function is discretized on a number of points sufficient to enable the convergence of the physical quantities such as density, thermal energy, and acoustic speed. In most of the simulations shown in this paper, we used $n=30$ points, with $v_0=0$ and $v_{n-2}=6v_{\mathrm{th}0}$ at $t=0$, while the last velocity is considered to be infinite, $v_{n-1}=\infty$, with $f_{n-1}=0$, the last temperature conserving its initial value $T_{n-2}=T_{e0}$ at any time (this assumption will be justified later).

The expression for the distribution function allows us to compute analytically some quantities needed to integrate numerically the Poisson equation. The electron density is calculated by simply integrating the distribution,

$$n_e(x,t) = 2\left(\sum_{j=k}^{\infty} \alpha_j \int_{u_j}^{u_{j+1}} F_j dv + \alpha_{k-1} \int_0^{u_k} F_{k-1} dv\right), \quad (31)$$

where u_k is defined as the first $u_j \in \mathbb{R}$. Using the error function erf, the density reads

$$n_e(x,t) = \frac{n_{e0}}{v_{\text{th}0}}\left[\sum_{j=k}^{\infty} \beta_j \exp\left(\frac{e\Phi}{k_B T_j}\right) + \beta^* \exp\left(\frac{e\Phi}{k_B T_{k-1}}\right)\right], \quad (32)$$

with

$$\beta_j = \alpha_j v_{\text{th}j}\left[\text{erf}\left(\frac{u_{j+1}}{\sqrt{2}v_{\text{th}j}}\right) - \text{erf}\left(\frac{u_j}{\sqrt{2}v_{\text{th}j}}\right)\right],$$

$$\beta^* = \alpha_{k-1} v_{\text{th}_{k-1}} \text{erf}\left(\frac{u_k}{\sqrt{2}v_{\text{th}_{k-1}}}\right).$$

Knowing the electron density as a function of Φ, we can determine the expression for the electric field at the ion front, E_f, at any time. Integration of the Poisson equation in the pure electron cloud from x_f to ∞ gives

$$\begin{aligned}\frac{\epsilon_0 E_f^2}{2} &= e\int_{\Phi_f}^{-\infty} n_e(\Phi) d\Phi \\ &= \frac{e n_{e0}}{v_{\text{th}0}}\left[\sum_{j=k}^{\infty} \int_{\Phi_f}^{-\mathcal{E}_j} \beta_j \exp\left(\frac{e\Phi}{k_B T_j}\right) d\Phi\right] \\ &\quad + \int_{\Phi_f}^{-\mathcal{E}_k} \beta^* \exp\left(\frac{e\Phi}{k_B T_{k-1}}\right) d\Phi, \end{aligned} \quad (33)$$

where Φ_f is the electric potential at the ion front. The electric field at the front can be hence written

$$E_f = \left[\frac{2n_{e0}}{\epsilon_0 v_{\text{th}0}}\left(\sum_{j=k}^{\infty} \alpha_j v_{\text{th}j}(\mathcal{K}_j^{j+1} - \mathcal{K}_j^j) + \alpha_{k-1} v_{\text{th}_{k-1}} \mathcal{K}_{k-1}^k\right)\right]^{1/2}, \quad (34)$$

where

$$\mathcal{K}_j^l = e\int_{\Phi_f}^{-\mathcal{E}_l} \text{erf}\left(\frac{u_l}{\sqrt{2}v_{\text{th}j}}\right)\exp\left(\frac{e\Phi}{k_B T_j}\right) d\Phi \quad (35)$$

$$\begin{aligned} &= k_B T_j\left[\sqrt{\frac{2}{\pi}}\frac{u_l(\Phi_f)}{v_{\text{th}j}}\exp\left(-\frac{\mathcal{E}_l}{k_B T_j}\right)\right. \\ &\quad \left. - \text{erf}\left(\frac{u_l(\Phi_f)}{\sqrt{2}v_{\text{th}j}}\right)\exp\left(\frac{e\Phi_f}{k_B T_j}\right)\right]. \end{aligned} \quad (36)$$

Finally, the calculation of the potential (or the field) in the hot electron cloud, $x \geq x_f$, is obtained by changing in the expression (33) the integral boundary Φ_f by Φ.

At time $t=0$, one has $\alpha_j=1$, $v_{\text{th}j}=v_{\text{th}0}$, and $T_j=T_{e0}$, which implies $n_e(x,0)=n_{e0}\exp(e\Phi/k_B T_{e0})$ as wanted. Similarly, the expression (34) reduces to [20] $E_f=(2/e_N)^{1/2}E_0$, with $e_N=2.718\,28\ldots$ and $E_0=(n_{e0}k_B T_{e0}/\epsilon_0)^{1/2}$.

C. Numerical method of integration

The set of equations (10), (21), (22), and (24) is solved with a global iterative method. More precisely guessed values of the velocities $v_j(t)$ are first obtained by extrapolation at time t from their values at the previous time steps. The Poisson equation is then linearized around a guessed value of the electric potential, which is simply its value at the previous time step. Solving this linearized Poisson equation gives a new value of the potential, which is used to compute the energy loss of the electrons. This in turn leads to corrected values of the velocities $v_j(t)$. The procedure is then iterated a few times, and we have verified its rapid convergence in fewer than ten iterations. Once the electric potential is determined, the ions are moved according to Eq. (21).

The time step Δt is governed by the ion dynamics and is chosen as a fraction of the inverse of the ion plasma frequency $\omega_{pi}=(Z^2 n_{i0}e^2/m_i\epsilon_0)^{1/2}$. The results presented in this paper were obtained with $\omega_{pi}\Delta t=0.2$. Typically we follow about 10^3 ions. The vacuum, which is explored by most energetic electrons, is treated with an adaptative mesh dependent on the local Debye length, with up to a few thousand points.

IV. NUMERICAL RESULTS AND COMPARISONS WITH PIC SIMULATIONS

We present in this section some results of our hybrid kinetic code. In order to check the validity of the model, the results will be compared with the ones obtained with the hybrid model described in Ref. [28], which assumes a time-dependent Maxwellian distribution, and the ones obtained with a one-dimensional PIC code.

The PIC code is nonrelativistic and purely electrostatic. As in the kinetic model, the ions initially occupy a slab of thickness L, while the electrons are in Maxwell-Boltzmann equilibrium with the self-consistent electrostatic potential, with a Debye sheath in vacuum on both sides. The mass ratio is $m_i/m_e=1836$, with $Z=1$, and initially $T_{e0}/T_{i0}=1000$. The simulation box is about $3\times10^4\lambda_{D0}$ long where $\lambda_{D0}=(\epsilon_0 k_B T_{e0}/n_{e0}e^2)^{1/2}$. There are 4×10^5 particles in each mesh, with $\Delta x=0.2\lambda_{D0}$. The PIC code is running with a time step of $\omega_{pe}\Delta t=0.05$, where ω_{pe} is the electron plasma frequency.

A. Velocity distribution

Figure 3 shows the velocity distribution in the center of the plasma foil, where the electric potential vanishes, at time $\omega_{pi}t=30$ and $\omega_{pi}t=100$ for a plasma slab of initial thickness $40\lambda_{D0}$. The distribution in any position x can be deduced from the distribution in the center of the foil by shifting the energy by the potential energy $-e\Phi(x,t)$. One can see the very good agreement between the results of the kinetic model and of the PIC simulations. The small fluctuations that we can notice in the PIC distribution for high velocities come from the very low amount of macroparticules in this phase space region.

The Maxwellian distribution corresponding to the temperature computed in the hybrid model [28] is plotted in

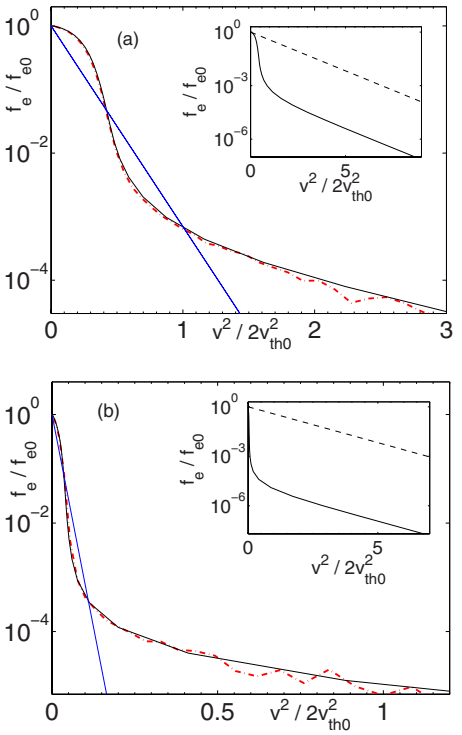

FIG. 3. (Color online) Velocity distribution at (a) $\omega_{pi}t=30$ for $L/2=20\lambda_{D0}$ and (b) $\omega_{pi}t=100$. Black line, kinetic model; red dash-dotted line, PIC code; blue straight line, hybrid model of Ref. [28] (time-dependent Maxwellian distribution). The dashed line in the inset represents the initial velocity distribution. The distributions are normalized to $f_e(0,0,0)$ and are taken at the center of the plasma foil, $x=0$.

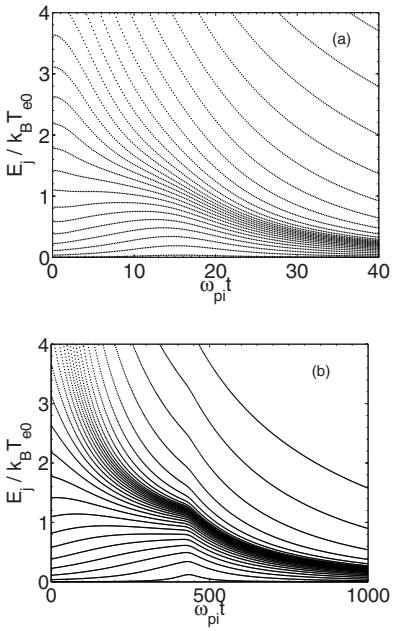

FIG. 4. Kinetic energy characteristics for (a) $L/2=20\lambda_{D0}$ and (b) $L/2=500\lambda_{D0}$.

blue. While the energy contents of the distribution functions given by the three models are in fact very close, as we will see later, one observes a strong departure of the actual distribution function (given either by the kinetic or the PIC models) with respect to the Maxwellian distribution, with a larger number of low-energy electrons, a smaller number of intermediate-energy electrons, and finally a larger number of high-energy electrons. The two first behaviors are consistent with the discussion given in Sec. II C 2, indicating the initial tendency of the electron distribution function to evolve toward a top-hat distribution. The high-energy part, not predicted by the discussion of Sec. II C 2, is in fact related to the non-neutral outer part of the electron cloud expansion in vacuum.

Figure 4 shows the time evolution of the total energy $\mathcal{E}_j$ of the electrons describing the electron distribution function for $L=40\lambda_{D0}$ and $L=1000\lambda_{D0}$. As discussed in Sec. II C 2, low-energy electrons $[\mathcal{E}_j(t=0)<3k_BT_{e0}/2$ in the large-L limit] gain energy during the first phase of the expansion, while high-energy electrons lose energy. After a time corresponding approximately to $L/2c_{s0}$, where $c_{s0}=(Zk_BT_{e0}/m_i)^{1/2}$, all the electrons eventually lose energy. Note that, as will be discussed later in Sec. IV D, this time is the time at which the ion rarefaction wave reaches the center of the foil.

By varying L, we have verified that the whole structure of the characteristics $\mathcal{E}_j(t)$ tends to a self-similar behavior when time is scaled to L. The departure from the self-similar character is due to higher-energy electrons which reach the vacuum region. Note that the characteristics of these high-energy electrons seem to be regularly spaced out. It is due to the fact that they experience an energy loss which does not depend on their energy, as already observed in Fig. 3, which shows that the hot tail of the velocity distribution remains Maxwellian with the initial temperature T_{e0}. The velocity distribution of high-energy electrons $(\mathcal{E}\gg|e\Phi_f|)$ can be written in the form

$$f_{eh}(\mathcal{E}) \propto e^{-\mathcal{E}/k_BT_{e0}}. \tag{37}$$

Consequently, we can assume that the potential in the pure hot electron cloud can be written roughly as in the isothermal model [20],

$$\Phi(x,t) \simeq \Phi_f - 2k_BT_{e0}\ln\left(1+\frac{x-x_f}{(2e_N)^{1/2}\lambda_{Dhf}}\right), \tag{38}$$

where $\lambda_{Dhf}=(\epsilon_0k_BT_{e0}/n_{ef}e^2)^{1/2}$. One can hence estimate the energy variation rate for high-energy electrons, for which most of the energy losses occur in the pure electron cloud. One obtains

$$\left\langle\frac{d\mathcal{E}}{dt}\right\rangle = -e\left\langle\frac{\partial\Phi}{\partial t}\right\rangle \simeq -e\left(\frac{d\Phi_f}{dt}-\frac{k_BT_{e0}}{n_{ef}}\frac{dn_{ef}}{dt}\right), \tag{39}$$

where we have used the expression for $\partial\Phi/\partial t$ corresponding to $x\gg x_f$, which is independent of space. Figure 5 shows a good agreement between the analytical expression (39) and the numerical results.

B. Phase space evolution

To show the evolution of the distribution function, we have chosen a plasma slab half-width of $L/2=20\lambda_{D0}$. The distribution function in the phase space is shown in Fig. 6 for

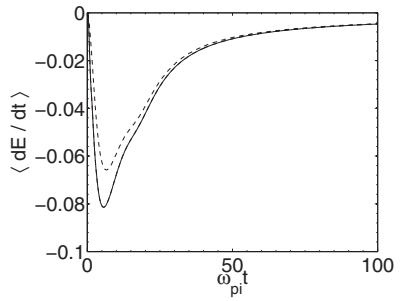

FIG. 5. Energy variation rate for high-energy electrons (hot tail of the velocity distribution). Black line, numerical result; dashed line, analytical result from expression (39).

$\omega_{pi}t=0, 10$, and 30. The distribution function is normalized to its initial value in the center of the target, $f_{e0}=f_e(0,0,0)$, and only one-quarter of the phase space is represented, due to the symmetry of the expansion. The phase space is represented by the isocontours of the distribution which are displayed in a color scale for the PIC results and with black lines for the kinetic model. The values of the distribution function in the center of the target, f_j, has been chosen to correspond to the logarithmic color scale of the PIC datas to facilitate the comparison. Note that the isocontours may also be interpreted as the electron trajectories in the phase space, due to the slow time variation of the potential. Actually, in order to compare results from both codes, the mean electronic velocity (first moment of the distribution) has been subtracted in the PIC results since our discrete distribution only depends on the energy of the electrons and therefore does not include the mean velocity. As a result, one can see in the figures the excellent agreement between the PIC and the kinetic isocontours. For $\omega_{pi}t=10$ ($\omega_{pi}t=30$) the ion front is located at $x_f \simeq 45\lambda_{D0}$ ($x_f \simeq 140\lambda_{D0}$), and manifests itself by a bump on the isocontours.

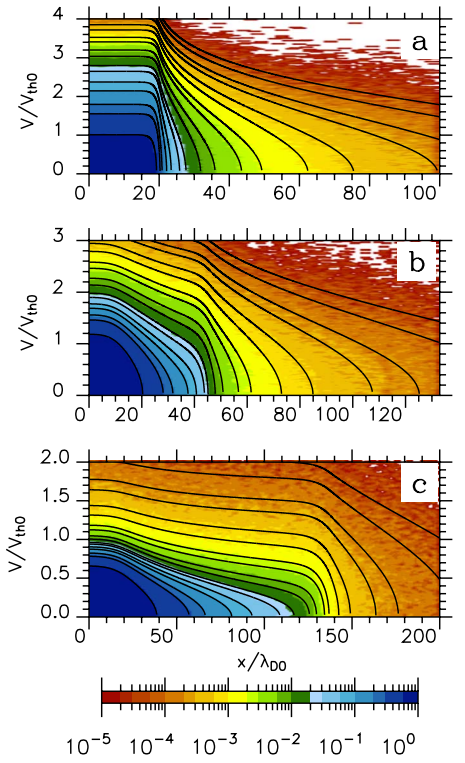

FIG. 6. (Color online) Isocontours of the electron distribution function in the phase space at $\omega_{pi}t=$ (a) 0, (b) 10, and (c) 30. PIC and kinetic results are shown, respectively, with a logarithmic color scale and with black lines. Note that the scales are different for each picture (though the surface of the displayed phase space is kept constant).

C. Thermal energy

One can calculate in our kinetic model the thermal energy density of the electrons

$$\mathcal{D}_{\rm th}(x,t) = \frac{m_e}{2}\int_{-\infty}^{\infty} v^2 f_e(x,v,t)dv. \tag{40}$$

With the distribution defined in Eq. (24), one obtains

$$\mathcal{D}_{\rm th} = \frac{m_e n_{e0}}{\sqrt{2\pi}v_{\rm th0}}\left[\sum_{j=k}^{\infty}\sigma_j \exp\left(\frac{e\Phi}{k_B T_j}\right) + \sigma^* \exp\left(\frac{e\Phi}{k_B T_{k-1}}\right)\right], \tag{41}$$

with

$$\sigma_j = \alpha_j v_{{\rm th}j}^2\left\{\sqrt{\frac{\pi}{2}}v_{{\rm th}j}\left[\mathrm{erf}\left(\frac{u_{j+1}}{\sqrt{2}v_{{\rm th}j}}\right) - \mathrm{erf}\left(\frac{u_j}{\sqrt{2}v_{{\rm th}j}}\right)\right] - \left[u_{j+1}\exp\left(-\frac{u_{j+1}^2}{2v_{{\rm th}j}^2}\right) - u_j \exp\left(-\frac{u_j^2}{2v_{{\rm th}j}^2}\right)\right]\right\},$$

$$\sigma^* = \alpha_{k-1}v_{{\rm th}_{k-1}}^2\left[\sqrt{\frac{\pi}{2}}v_{{\rm th}_{k-1}}\mathrm{erf}\left(\frac{u_k}{\sqrt{2}v_{{\rm th}_{k-1}}}\right) - u_k \exp\left(-\frac{u_k^2}{2v_{{\rm th}_{k-1}}^2}\right)\right].$$

One can define the local temperature $T(x,t) = 2\mathcal{D}_{\rm th}(x,t)/n_e(x,t)k_B$. This function is shown in Fig. 7(a) as a function of space for three different times. The temperature first decreases, then increases, and asymptotically reaches the initial temperature T_{e0} for $x\to\infty$. This behavior can easily be deduced from the analysis of the distribution function in the center of the foil [Fig. 3].

One can also determine the mean thermal energy per electron $\langle\mathcal{E}_{\rm th}\rangle = \int\mathcal{D}_{\rm th}dx/N_e$, where $N_e=\int f_e dv\,dx$ represents the total number of electrons (per unit surface). The mean thermal energy is shown in Fig. 7(b) and compared with the results of the PIC code and of the hybrid model of Ref. [28]. We can notice that the results from the three models coincide almost exactly. We find again the asymptotic law obtained in the hybrid model $\langle\mathcal{E}_{\rm th}\rangle \propto t^{-2}$.

D. Ion acoustic speed and disassembly time

The disassembly time can be defined as the time taken by the rarefaction wave, traveling at the ion acoustic speed, to reach the center of the foil. Assuming as a first approximation that the temperature does not change significantly during

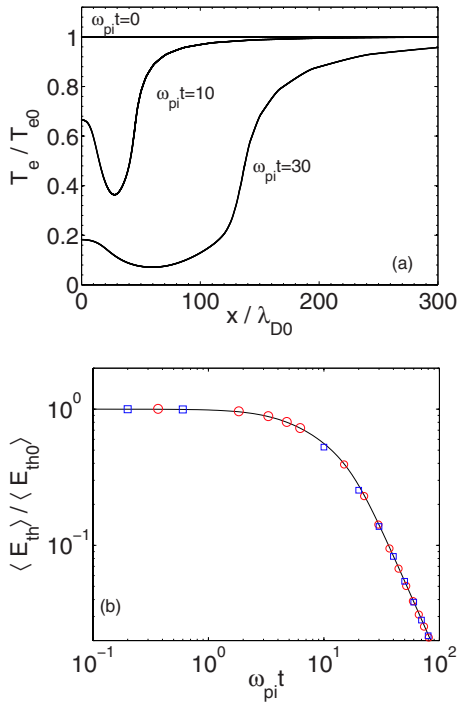

FIG. 7. (Color online) (a) Temperature as a function of space. (b) Time evolution of the mean thermal energy. The results of the kinetic model, PIC simulation, and hybrid model are plotted, respectively, as solid line, red circles, and blue squares.

this phase, the disassembly time is roughly given by $t_{d0} \sim L/2c_{s0}$ [28]. Actually, in the hybrid model of Ref. [28], the ion acoustic speed is decreasing with time as $\sqrt{T_e}$ and the disassembly time is slightly larger than t_{d0}. In contrast, we show here that, though the mean electron energy is a decreasing function of time, the ion acoustic velocity inside the inner part of the slab is in fact increasing with time during the first phase of the expansion. This strongly counterintuitive result is related to the strong departure of the electron distribution function with respect to a Maxwellian distribution of the same mean energy. To prove this assertion, let us calculate the time evolution of the acoustic speed in the kinetic theory.

To determine the ion acoustic speed, we consider an ion perturbation of characteristic wave number k (strictly speaking, k should verify $\lambda_{D0} \ll k^{-1} \ll L$). The corresponding dispersion relation for the acoustic wave in kinetic theory is known to be

$$\frac{\omega^2}{\omega_{pi}^2} = \frac{m_e k^2 \epsilon_0}{e^2} \left(\int_{-\infty}^{\infty} \frac{\partial f_{e0}}{\partial v} \frac{dv}{v} \right)^{-1}. \tag{42}$$

In the expansion, the electron distribution function is distorted from the initial Maxwell-Boltzmann distribution and the dispersion relation (42) has to be evaluated with the (slowly) time-varying distribution function f_{e0} as in the quasilinear theory. The distribution is taken at the center of the foil, $f_{e0}=f_e(x=0,v,t)$, since the rarefaction wave is traveling in the inner part of the plasma slab during the first phase of the expansion.

With the distribution function (24), the dispersion relation reduces to

$$\frac{\omega^2}{\omega_{pi}^2} = \frac{k^2 \lambda_{D0}^2}{C_\Sigma}, \tag{43}$$

with

$$C_\Sigma = \sum_{j=0}^{\infty} C_j \exp\left(\frac{e\Phi}{k_B T_j} \right) \tag{44}$$

and

$$C_j = \frac{\alpha_j v_{\text{th}0}}{v_{\text{th}j}} \left[\text{erf}\left(\frac{u_{j+1}}{\sqrt{2} v_{\text{th}j}} \right) - \text{erf}\left(\frac{u_j}{\sqrt{2} v_{\text{th}j}} \right) \right].$$

The expression (43) is in fact valid at any time, not only during the first phase of the expansion. Thus it is necessary to take into account the ion density decreasing in the center of the foil at late times, so that the ion acoustic speed finally reads

$$c_s = c_{s0} \left(\frac{n_i(0,t)}{C_\Sigma n_{i0}} \right)^{1/2}. \tag{45}$$

Figure 8(a) shows the time evolution of the ion acoustic velocity in the center of the slab. Also shown is the quantity $[Zk_BT(0,t)/m_i]^{1/2}$ which represents the ion acoustic speed of a Maxwellian distribution of the same energy content. As said before, the ion acoustic velocity is first increasing with time, while the energy content is decreasing.

The position of the rarefaction front as a function of time is $x_{\text{rar}}(t) \simeq x_{\text{rar}}(0) - \int_0^t c_s(t')dt'$ (in practice the rarefaction front has a spatial extension of a few Debye lengths). The disassembly time is hence given by the equation

$$L = 2\langle c_s \rangle t_d, \tag{46}$$

where $\langle c_s \rangle t_d = \int_0^{t_d} c_s dt$. Numerically we obtain $\langle c_s \rangle \simeq 1.14 c_{s0}$ and $t_d \simeq (7/8) t_{d0}$.

To illustrate the effect of the departure from a Maxwellian, let us consider super-Maxwellian distributions of the form

$$f_e(v) = \frac{n}{2\Gamma(1/n)} \left(\frac{n_{e0}}{v_0} \right) \exp - \left(\frac{v}{v_0} \right)^n, \tag{47}$$

with

$$v_{\text{th}0} = \left(\frac{\int v^2 f_e dv}{n_{e0}} \right)^{1/2} = v_0 \left(\frac{\Gamma(3/n)}{\Gamma(1/n)} \right)^{1/2}, \tag{48}$$

where Γ is the usual Gamma function. Using (42), the ion acoustic speed reads

$$c_s = c_{s0} \frac{\Gamma(1/n)}{[n\Gamma(3/n)\Gamma(1-1/n)]^{1/2}}, \tag{49}$$

where $c_{s0} = (Zm_e/m_i)^{1/2} v_{\text{th}0}$.

Figure 8(b) shows the ion acoustic velocity as a function of n for a distribution function of the form (47). Also shown in Fig. 8(c) is the value $n(t)$ for which the ratio c_s/c_{s0} de-

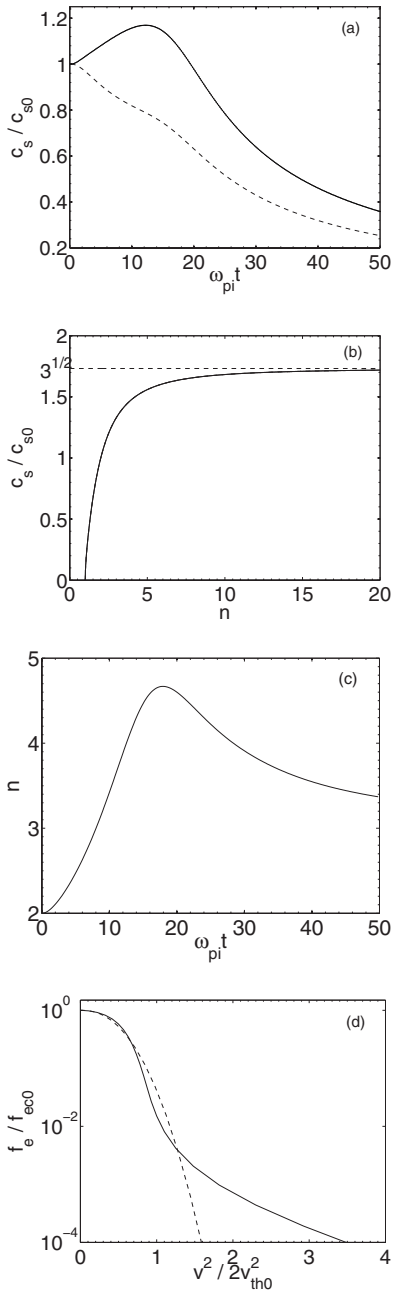

FIG. 8. (a) Ion acoustic velocity as a function of time at position $x=0$. Also shown as the dashed line is the quantity $[Zk_BT(0,t)/m_i]^{1/2}$ normalized to c_{s0}. (b) Ion acoustic speed as a function of n for super-Maxwellian distribution of the form (47). (c) n as a function of time as deduced from the comparison of (a) and (b). (d) Distribution function for $\omega_{pi}t=20$ and its fit (dashed line) by a super-Maxwellian with $n=4.6$.

duced from Fig. 8(a) coincides with the ratio effectively observed in Fig. 8(a). Figure 8(d) shows an example of such a fit, for $\omega_{pi}t=20$.

E. Spatial profiles

The spatial profiles of the potential, the electric field, the ion density, and the electron and ion mean velocities are plotted in Figs. 9 and 10 for the kinetic, the PIC, and the hybrid models, at $\omega_{pi}t=30$. One can verify in Fig. 9(a) that the electric potential behavior in vacuum in the kinetic and PIC calculations is correctly given by Eq. (38). On the other hand, though the hybrid model predicts the correct value of the potential at the position of the ion front, its description of the vacuum appears quite poor, essentially because it does not take into account the spatial structure of the temperature as shown in Fig. 7(a).

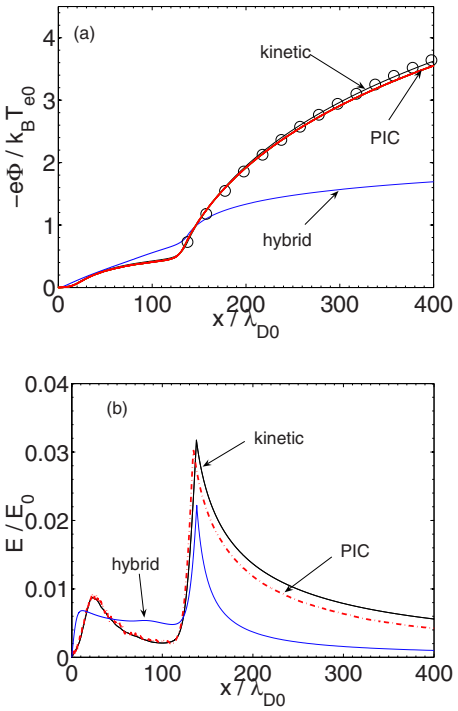

FIG. 9. (Color online) (a) Spatial profile of the electrostatic potential for the kinetic (black line), the PIC (red dashed-dotted line), and the hybrid (blue line) models at $\omega_{pi}t=30$. (b) Corresponding spatial profile of the electric field. Also shown in black circles, the potential of the formula (38).

One also notes the excellent agreement of the electric field predicted by the kinetic and the PIC models in Fig. 9(b). On the other hand, slight discrepancies appears at late times with the hybrid model. Although the position of the electric field peak (at the ion front) is consistently predicted by the three models, its magnitude and width are larger in the kinetic and PIC models than in the hybrid model. This feature was in fact already present in Fig. 3 of Ref. [34]. As a matter of fact, the width and the magnitude of the peak of the electric field are mainly determined by the local temperature at the ion front x_{front} via the local Debye length. In the kinetic and PIC models, the local temperature satisfies $2\langle\mathcal{E}_{\text{th}}\rangle/k_B < T(x_{\text{front}},t) < T_{e0}$, while in the hybrid model [28] the ion front temperature almost coincides with the averaged temperature $2\langle\mathcal{E}_{\text{th}}\rangle/k_B$.

The ion density profiles, shown in Fig. 10(a) at $\omega_{pi}t=30$, are similar in the three models. However we note that the ion density in the center of the foil is lower in the kinetic and PIC models than in the hybrid model. Indeed, this is due to the fact that, as explained in Sec. IV D, the rarefaction wave is reaching the center of the foil earlier in the kinetic and PIC models.

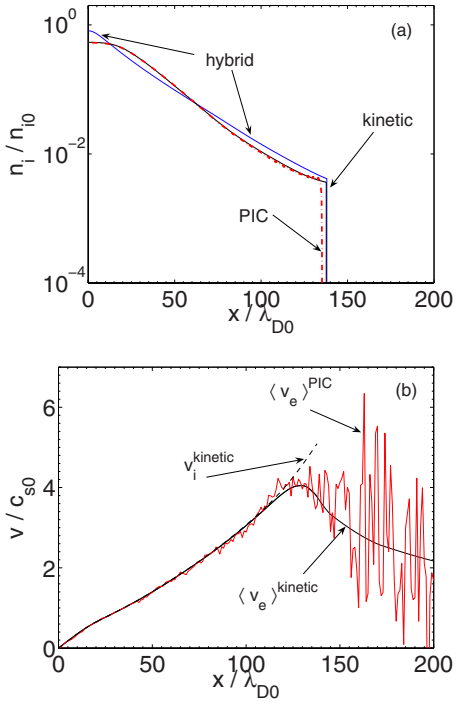

FIG. 10. (Color online) (a) Spatial profile of the ion density at $\omega_{pi}t=30$ for the kinetic (black line), PIC (red line), and hybrid (blue line) models. (b) Spatial profile of the mean ion (black dashed line) and electron velocities for the kinetic (black line) and PIC (red line) models.

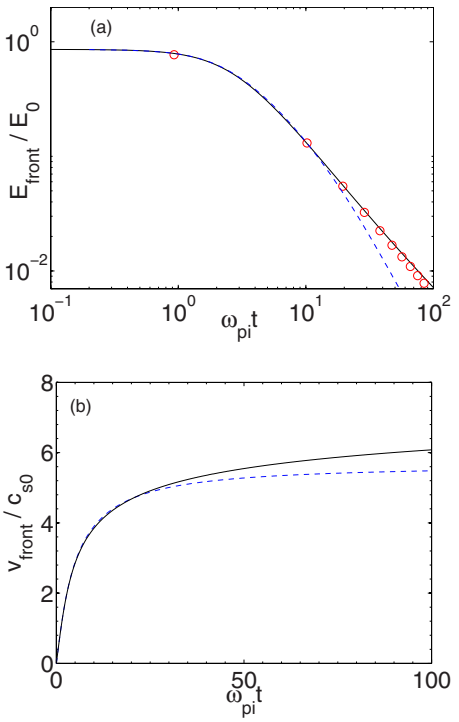

FIG. 11. (Color online) (a) Time evolution of electric field at the ion front for the kinetic (black line), PIC (red circles), and hybrid (blue dashed line) models. (b) Time evolution of the ion velocity at the ion front for the kinetic (black line) and hybrid (blue dashed line) models.

The last remark concerns the mean electron velocity which cannot be calculated with our distribution. It is nevertheless possible to obtain the electron mean velocity with the Maxwell-Ampère equation without magnetic field ($\nabla \times \mathbf{B} = \mathbf{0}$),

$$v_e = \frac{n_i}{n_e} v_i + \frac{\epsilon_0}{e n_e} \frac{\partial E}{\partial t}. \tag{50}$$

By introducing the Lagrangian operator $d/dt = \partial/\partial t + v_i \partial/\partial x$, where v_i is the ion velocity in the plasma (for $x \leq x_f$) or the velocity of the numerical mesh in the vacuum (for $x > x_f$), and using the Poisson equation (22), one finds

$$v_e = v_i + \frac{\epsilon_0}{e n_e} \frac{dE}{dt}. \tag{51}$$

The electron mean velocity is plotted in Fig. 10(b) and is compared with the mean velocity obtained in the PIC code. Also shown is the ion velocity v_i for $x \leq x_f$. One can observe the good agreement of both codes in the plasma region. In the vacuum ($x > x_f$), the PIC code gives noisy results because of the very small number of particles per cell in this region, whereas our model provides a smooth plot of the mean electron velocity.

F. Final velocity

The values of the field in the three models are similar until the disassembly time, from which the asymptotic evolutions slightly differ, as can be seen in Fig. 11(a), which shows the time evolution of the field at the front in the three models. At late times the hybrid model predicts a fast decrease of the electric field at the ion front, $E_f = \sqrt{2} k_B T_e / e \lambda_{Df} \propto t^{-2}$, while the kinetic model as well as the PIC code predict $E_f \propto t^{-m}$ with $1 < m < 2$. This difference in the scaling laws is again due to the fact that the electron temperature at the ion front is smaller in the hybrid model than in the kinetic and PIC models.

A slower decrease of the field leads necessarily to a slower convergence of the front velocity as a function of time. This trend can be verified in Fig. 11(b), which shows the ion front velocity for the hybrid model [28] and for the present kinetic model. Note, however, that the two curves go apart at late times only, after most of the acceleration has taken place.

V. CONCLUSION

We have studied the one-dimensional expansion of a plasma slab into a vacuum with a kinetic description of the electron population. It has been shown that the slow time evolution of the self-consistent electrostatic potential allows one to carry out a separation between a slow time scale linked with the ion motion and a fast time scale corresponding to the electron transit time in the potential well. The adiabatic behavior of the electrons enables us to calculate their mean energy variation in the potential and hence to determine the electron distribution function at any time. We demonstrate that, due to the expansion, the electron velocity

distribution function does not remain Maxwellian. As a matter of fact, we notice that the distribution function in the center of the plasma slab is composed of two parts. The first part corresponds to electrons whose behavior is determined by the quasineutral plasma region with a time-decreasing mean energy. The second part corresponds to electrons that reach the outer purely electronic part of the system and maintain the initial slope of the distribution function. A special section has been devoted to the determination, in the central part of the slab, of the acoustic speed, which is also the rarefaction wave velocity. We have shown that, at least during the initial phase of the expansion, it accelerates due to the distortion of the distribution function, in contrast with the predictions of purely fluid models. The disassembly time of the plasma slab is hence smaller than expected. We have also observed that the acceleration of the ions during the expansion is more efficient at late times in the kinetic model than in the hybrid model. All of these observations are in full agreement with PIC simulations.

All the simulations shown in this paper correspond to an initial electron distribution function given by a Maxwellian distribution function. However, the model is not restricted to a particular form of the initial electron distribution function, and we have used it, for instance, with an initial distribution function given by the sum of two Maxwellian distributions (cold and hot electrons), similarly to what was done in the hybrid model of Ref. [28]. The model is able to treat realistic temperature and density ratios (up to hundreds or more). The presentation of the corresponding results is left for a future presentation.

The kinetic model presented in this paper is nonrelativistic. Its extension to the relativistic case is rather straightforward, as the adiabatic hypothesis used here still applies.

The kinetic study of plasma expansion presented in this paper is strictly one dimensional. The potential coupling with the transverse direction is not taken into account. Coupling might occur due to any source of angular redistribution of the electron energy. Collisions or electromagnetic instabilities are potential sources for such a coupling. Collisions might play an important role if the collision time is comparable to or smaller than the characteristic time $L/2c_{s0}$. Similarly, electromagnetic instabilities are expected to occur on characteristic times of the order of a few times the ratio of the skin depth c/ω_{pe} to the thermal velocity v_{te}, which is implicitly supposed here to be larger than $L/2c_{s0}$. The study of the coupling to transverse directions is left for future work.

ACKNOWLEDGMENT

This work was partly supported by Agence Nationale de la Recherche (ANR) Project No. ANR-06-BLAN-0392.

[1] E. L. Clark *et al.*, Phys. Rev. Lett. **84**, 670 (2000).
[2] A. Maksimchuk, S. Gu, K. Flippo, D. Umstadter, and V. Yu. Bychenkov, Phys. Rev. Lett. **84**, 4108 (2000).
[3] S. P. Hatchett *et al.*, Phys. Plasmas **7**, 2076 (2000).
[4] R. A. Snavely *et al.*, Phys. Rev. Lett. **85**, 2945 (2000).
[5] J. Badziak, E. Woryna, R. Parys, K. Y. Platonov, S. Jablonski, L. Ryc, A. B. Vankov, and J. Wolowski, Phys. Rev. Lett. **87**, 215001 (2001).
[6] A. J. Mackinnon, Y. Sentoku, P. K. Patel, D. W. Price, S. Hatchett, M. H. Key, C. Andersen, R. Snavely, and R. R. Freeman, Phys. Rev. Lett. **88**, 215006 (2002).
[7] M. Hegelich *et al.*, Phys. Rev. Lett. **89**, 085002 (2002).
[8] M. Allen *et al.*, Phys. Plasmas **10**, 3283 (2003).
[9] V. Yu. Bychenkov, V. T. Tikhonchuk, and S. V. Tolokonnikov, Sov. Phys. JETP **88**, 1137 (1999).
[10] Y. Sentoku *et al.*, Phys. Rev. E **62**, 7271 (2000).
[11] H. Ruhl, S. V. Bulanov, T. E. Cowan, T. V. Liseikina, P. Nickles, F. Pegoraro, M. Roth, and W. Sandner, Plasma Phys. Rep. **27**, 363 (2001).
[12] V. S. Khoroshkov and E. I. Minakova, Eur. J. Phys. **19**, 523 (1998).
[13] S. C. Wilks *et al.*, Phys. Plasmas **8**, 542 (2001).
[14] A. J. Mackinnon, M. Borghesi, S. Hatchett, M. H. Key, P. K. Patel, H. Campbell, A. Schiavi, R. Snavely, S. C. Wilks, and O. Willi, Phys. Rev. Lett. **86**, 1769 (2001).
[15] A. Pukhov, Phys. Rev. Lett. **86**, 3562 (2001).
[16] S. C. Wilks, W. L. Kruer, M. Tabak, and A. B. Langdon, Phys. Rev. Lett. **69**, 1383 (1992).
[17] T. Y. Brian Yang, W. L. Kruer, R. M. More, and A. B. Langdon, Phys. Plasmas **2**, 3146 (1995).
[18] W. Rozmus, V. T. Tikhonchuk, and R. Cauble, Phys. Plasmas **3**, 360 (1996).
[19] A. V. Gurevich, L. V. Pariiskaya, and L. P. Pitaevskii, Sov. Phys. JETP **22**, 449 (1966).
[20] J. E. Crow, P. L. Auer, and J. E. Allen, J. Plasma Phys. **14**, 65 (1975).
[21] P. Mora and R. Pellat, Phys. Fluids **22**, 2300 (1979).
[22] M. A. True, J. R. Albritton, and E. A. Williams, Phys. Fluids **24**, 1885 (1981).
[23] A. V. Gurevich and A. P. Meshcherkin, Sov. Phys. JETP **53**, 937 (1981).
[24] P. Mora, Phys. Rev. Lett. **90**, 185002 (2003).
[25] T. Grismayer and P. Mora, Phys. Plasmas **13**, 032103 (2006).
[26] D. S. Dorozhkina and V. E. Semenov, Phys. Rev. Lett. **81**, 2691 (1998); V. F. Kovalev, V. Yu. Bychenkov, and V. T. Tikhonchuk, Sov. Phys. JETP **95**, 226 (2002); V. F. Kovalev and V. Yu. Bychenkov, Phys. Rev. Lett. **90**, 185004 (2003).
[27] V. Yu. Bychenkov, V. N. Novikov, D. Batani, V. T. Tikhonchuk, and S. G. Bochkarev, Phys. Plasmas **11**, 3242 (2004).
[28] P. Mora, Phys. Rev. E **72**, 056401 (2005).
[29] A. V. Gurevich, Sov. Phys. JETP **26**, 575 (1968).
[30] F. Peano, R. A. Fonseca, and L. O. Silva, Phys. Rev. Lett. **94**, 033401 (2005); F. Peano, G. Coppa, F. Peinetti, R. Mulas, and L. O. Silva, Phys. Rev. E **75**, 066403 (2007); F. Peano, J. L. Martins, R. A. Fonseca, L. O. Silva, G. Coppa, F. Peinetti, and R. Mulas, Phys. Plasmas **14**, 056704 (2007).
[31] P. Mora, Phys. Plasmas **12**, 112102 (2005).
[32] L. D. Landau and E. N. Lifshitz, *Mechanics*, 3rd ed. (Butterworth-Heinemann, Oxford, 1976).
[33] A. V. Baitin and K. M. Kuzanyan, J. Plasma Phys. **59**, 83 (1998).
[34] L. Romagnani *et al.*, Phys. Rev. Lett. **95**, 195001 (2005).